

A Universal Quantum Electron Microscope for Phase Objects: Hardware Designs and Possible Applications

Hiroshi Okamoto^{1,*}

¹*Department of Intelligent Mechatronics, Akita Prefectural University, Yurihonjo 015-0055, Japan*

(Dated: September 13, 2022)

We present simple designs of a quantum electron microscope that is capable of performing any multi-pixel quantum operations, provided that the specimen is a phase object. The designs are intended for quantum-enhanced measurement of beam-sensitive specimens. A possible application of such a microscope is the Grover search for a structure, out of a set of candidate structures.

Quantum query complexity is the number of calls a quantum computer needs to make to an “oracle” to solve a problem [1]. The query model has been extensively studied in the field of quantum computing because it is relevant to many quantum algorithms and it also makes certain theoretical analyses tractable.

In a sense, the abstract concept of quantum query complexity becomes “real” in quantum measurement of fragile specimens. Specifically in the context of high-resolution biological electron microscopy (EM) [2], each query to the biological specimen, i.e., passing of a probe electron, may damage the specimen. Hence, in principle, low query complexity of a quantum algorithm designed to obtain information about the “oracle”, namely the specimen, translates to a measurement associated with a small amount of specimen damage. This in turn means that a large amount of information is obtainable from the specimen before we destroy it. Thus, query complexity is the figure of merit of an algorithm designed for a given task in this context, rather than a proxy for more fundamental measures of quantum advantage, such as the time complexity.

An EM capable of querying the specimen in the above general sense has hardly been considered [3, 4]. On the other hand, the use of quantum enhancement in EM, in order to image beam-sensitive specimens, has been discussed for more than a decade [5–7] and also experimental efforts have begun to be reported [8, 9]. The putative, quantum-enhanced form of EM is often referred to as quantum electron microscopy (QEM). Many, though not all, proposals of QEM aim at imaging weak phase objects beyond the shot noise limit to approach the Heisenberg limit [10, 11]. Note that biological specimens are usually regarded as weak phase objects in EM.

In this Letter, we present designs of a *universal* QEM, which is able to perform anything programmable quantum mechanically. Universal QEM would make most sense when we perform tasks other than the standard phase contrast imaging. We will find that those other tasks may include efficiently finding a known pattern. Such measurements could indeed make sense in structural biology: Due to the recent developments in electron

cryomicroscopy (cryoEM), now we are largely able to determine atomic structures of biological molecules by *classical* averaging methods such as single particle analysis, provided that a large number of the molecule of interest are available [12]. In contrast, quantum enhancement is required when only a single copy of the specimen is available. Tasks such as comprehensively identifying *known* species of molecules in the crowded cellular environment, perhaps in the context of electron cryotomography [13], may be a suitable arena for quantum technologies.

From the fundamental perspective, universal QEM definitely is possible. One could, in principle, connect an EM to a quantum computer (QC) via suitable quantum interfaces [3] placed at both the illumination and detection sides of the EM. In this way, one could transfer, or teleport, a quantum state from the QC to the illuminating electron wave to the specimen and also transfer the state of the exit electron wave back to the QC. The real question, on the other hand, is whether there exists a sufficiently simple and feasible scheme to do so. We answer this question in the affirmative, on the condition that the specimen is a pure phase object. In what follows, the symbol e denotes the positron charge. Let the z -axis be the electron-optical axis. Let λ be the wavelength of imaging electrons. A *diffraction plane* is any plane conjugate to the back focal plane of the objective lens. An *image plane* refers to any plane conjugate to the plane where the specimen is placed. We will often omit the overall normalization factor of a quantum state.

Figure 1 shows our universal QEM scheme at the conceptual level. We defer discussions of physical realizations to later parts of this paper. At first glance, it is rather similar to the 4-dimensional (4D) scanning transmission EM (STEM) [14]. Following the electron gun and the condenser lens, there are two beam deflectors for bending the electron beam in the x and y directions at a diffraction plane. Below the pre- and post-field objective lens and the specimen, a pixelated electron detector is placed at a diffraction plane. The crucial difference from the conventional STEM, however, is that the beam deflector is quantum. Consider the beam deflector along the x -direction. This deflector is a qudit, i.e., a d -level quantum system, with d distinct quantum states $|0\rangle, |1\rangle, \dots, |d-1\rangle$. These states are associated with a set of correspondingly equally-spaced amount of magnetic flux, which bends the electron beam. A superconducting

*okamoto@akita-pu.ac.jp

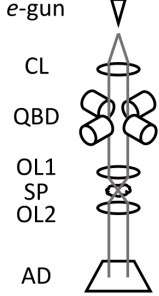


FIG. 1: Schematic drawing of a universal QEM at the conceptual level. It comprises a pulsed electron gun (e-gun), condenser lens (CL), quantum beam deflector (QBD), objective pre-field lens (OL1), specimen (SP), objective post-field lens (OL2), and a pixelated area detector (AD). Additional lenses, such as a projector lens, are not shown. To fully combat inelastic scattering events, an energy-dependent beam separator and another AD are required.

flux qubit [15], for example, is a $d = 2$ version of it. The same applies to the deflector in the y -direction. These two qudits, which we call qudit x and qudit y , are part of a larger quantum computer, equipped with as many additional qubits as necessary, that controls the QEM. Entanglement-assisted QEM [10] may be considered as a single-qubit version of the present scheme, without a QC.

The effect of the quantum beam deflectors is the following. Reflecting the $d \times d$ distinct quantum states of the combined system of qudits x and y , there correspond $d \times d$ points on the specimen, where the electron beam is focused. Hence one may raster-scan the electron beam by properly setting each qudits at proper times. What is newly enabled, however, is that one could also make a quantum superposition of various positions of the electron beam. Indeed, an arbitrary 2D pattern of the electron beam may be generated, although it is not exactly an arbitrary shape of the electron wave front, because the electron state is heavily entangled with the two qudits. Nonetheless, it is rather remarkable that an arbitrary 2D pattern can be generated by only two deflectors along the x and y directions. The ability of the two qudits to have entanglement between them enables this, and shows that a quantum instrument could, in a sense, occasionally be simpler than the classical counterpart.

Next, we show that our scheme is universal. Since the universality of the quantum computing part is trivially satisfied by the use of a QC, we consider the “oracle” call part. We want to probe the phase shift of the phase object at the $d \times d$ locations quantum mechanically. Let these locations be indexed by two integers p and q , where $0 \leq p < d$ and $0 \leq q < d$. Let the phase shift of the specimen at the location (p, q) be $\theta_{p,q}$. We define what we want as the result of an oracle call as

$$|p, q\rangle \Rightarrow e^{i\theta_{p,q}}|p, q\rangle, \quad (1)$$

for a quantum register $|p, q\rangle$ with d^2 states in our QC.

(Here we somewhat enlarge the notion of the oracle from the one used in computer science, wherein $\theta_{p,q}$ is restricted to be either 0 or π . Note that the latter can simulate the more widely used oracle that flips an ancilla qubit if and only if $\theta_{p,q} = \pi$.) The quantum register $|p, q\rangle$ turns out to be the combined qudits x and y : We let $|p, q\rangle = |p\rangle \otimes |q\rangle$, where $|p\rangle$ and $|q\rangle$ are the states of qudits x and y , respectively. To realize the transform of Eq. (1), we first produce an electron from the electron gun in the state $|0\rangle$, so that the initial state of the combined system of the electron and the beam deflector is $|0\rangle \otimes |p, q\rangle$. Let the electron state $|n, m\rangle$ be the one that is to be focused on the location (n, m) of the specimen. The action of the beam deflector is, by definition, $|0\rangle \otimes |p, q\rangle \Rightarrow |p, q\rangle \otimes |p, q\rangle$. Next, we let the electron pass the specimen. By definition, we obtain $|p, q\rangle \otimes |p, q\rangle \Rightarrow e^{i\theta_{p,q}}|p, q\rangle \otimes |p, q\rangle$. Finally, we detect the electron in the far field. This basically means a measurement of the electron state in the Fourier-transformed basis $|k, l\rangle = \frac{1}{N} \sum_{p,q} e^{i\frac{kp+ld}{N}} |p, q\rangle$. Suppose that we detected the electron at the point (k, l) on the diffraction plane. This leaves the two qudits in the state

$$e^{i\theta_{p,q}}|p, q\rangle \otimes |p, q\rangle \Rightarrow e^{i\theta_{p,q}} \cdot e^{-i\frac{kp+ld}{N}} |p, q\rangle. \quad (2)$$

Since we know k and l from our measurement, we perform a phase shift operation to the qudits x, y to obtain the state $e^{i\theta_{p,q}}|p, q\rangle$, which is the right-hand side of Eq. (1).

We proceed to discuss physical realizations of our scheme. The only nonstandard part in the scheme is the quantum beam deflector, and we focus on the part for the x -axis, i.e., the qudit x . Among various physical platforms for quantum memories, superconducting quantum circuit is a natural fit because of its ability to produce a quantum-mechanically superposed electromagnetic field around it. In particular, the flux qubit can produce a superposition of two distinct amount of magnetic flux ϕ_A and ϕ_B . As shown below, the magnetic flux difference $\Delta\phi = \phi_A - \phi_B$ has to be about the magnetic flux quantum $\phi_0 = h/2e$, with a multiplicative factor of order 1 depending on detailed designs [16]. Figure 2 (a) shows a trajectory of an electron with a velocity v passing by a flux qubit, with the dimensions shown in the figure, which is bent depending on the qubit state. Since the electron wave has an angular spread $\approx \lambda/w$ after passing over the qubit due to diffraction, the angular deflection should satisfy

$$\frac{\Delta p}{p} = \frac{evB\Delta t}{p} = \frac{ev\phi}{plw} \cdot \frac{l}{v} = \frac{e\phi}{pw} > \frac{\lambda}{w} = \frac{h}{pw}, \quad (3)$$

where $p, \phi, B, \Delta t$ are, respectively, the momentum of the electron, the magnetic flux held by the qubit, the magnetic flux density and the time the electron takes to fly by the qubit. Hence we obtain the condition $\phi \gtrsim \phi_0$ to produce a quantum-mechanically distinct electron wave. Unfortunately, the magnetic flux held by a flux qubit is usually smaller than ϕ_0 [17]. A conceptually simple way to work around this problem is to make a row of multiple flux qubits, each with states $|0\rangle$ and $|1\rangle$, and entangle

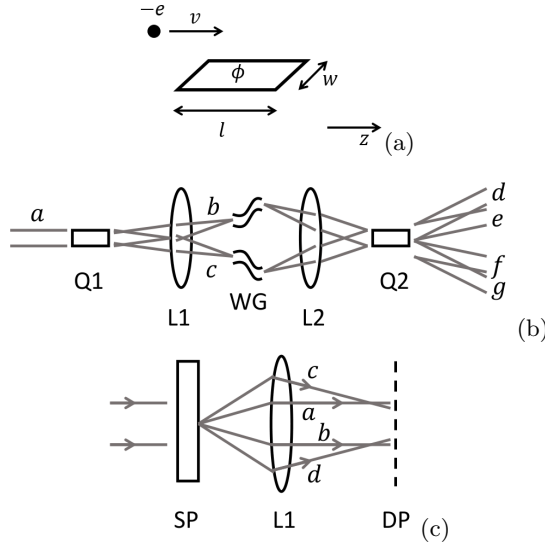


FIG. 2: Designs of some parts of the universal QEM. (a) An electron with a velocity v flies nearby a qubit with a trajectory parallel to the plane, on which the qubit is placed. The qubit, with the dimension $l \times w$, holds a magnetic flux ϕ . (b) A qudit comprising multiple qubits. Two qubits (Q_1, Q_2) placed on diffraction planes deflect the electron beam minimally. The lenses (L_1, L_2) separates the deflected electron waves on the image plane, where wave guides (WG) enlarges the separation between the two waves b and c . Q_1 deflects the incoming wave a into waves b and c depending on its state, and Q_2 deflects the waves b and c further into waves f, g and d, e , respectively. (c) Since the specimen (SP) is a phase object, the electron gets a phase shift upon transmission through the specimen (rays a and b). Some scattered waves with large scattering angles (rays c and d), however, have non-smooth wave intensity on the diffraction plane (DP) after going through the lens (L_1). This would adversely affect the quantum measurement. We merge rays c, d with rays a, b to avoid the adverse effect.

all of them so that, as a whole, the entire set of qubits operates in the space spanned by the states $|00 \dots 0\rangle$ and $|11 \dots 1\rangle$. This entire set of qubits may then be regarded as a single qubit with $\Delta\phi \approx \phi_0$, which we call a full-vortex qubit (FVQ). They could be realized either by brute-force applications of quantum gates to entangle all the constituent qubits, or by designing certain interaction among the constituent qubits [18]. One could then combine d FVQs to realize the qudit, although we will describe another way with $\ln d$ scaling shortly.

Another way for realizing a FVQ is the use of the so-called bosonic qubit [19]. A bosonic qubit can store, in its microwave cavity, microwave photons in a quantum-mechanically controlled fashion. A somewhat crude calculation [20] has shown that about α^{-1} photons, where α is the fine-structure constant, are needed to generate magnetic flux $\approx \phi_0$ in an instant when the photon energy is stored in the magnetic field. Since controlling ≈ 100 photons in a 3D cavity has been experimentally demonstrated [19], we can envision doing the same with a coplanar microwave cavity, above which an electron flies.

Figure 2 (b) shows a way to form a qudit using $\log_2 d$ qubits. These qubits form a quantum register to represent an integer $0 \leq p < d$ in the binary form. Assuming that each qubit can only bend the electron trajectory by the angle $\delta\theta \approx \lambda/w$, we need to artificially enlarge the deflection angle except for the least significant qubit. To do so, we separate the waves b, c from the qubit Q_1 by letting them go through the lens L_1 to arrive at an image plane. There we artificially enlarge the physical distance between the two waves by a classical means, most probably by an electromagnetic field. Indeed, highly versatile methods for electron wave manipulation have recently been reported [21, 22]. After going through L_2 to go to the next diffraction plane, the angle between the waves b, c is enlarged to be $2\delta\theta$, and hence Q_2 can split these waves into four waves d, e, f and g . A similar argument applies to a system comprising more than two qubits.

Three remarks are in order. Firstly, for 300 keV electrons and a typical dimension of microfabrication $w \approx 1 \sim 10 \mu\text{m}$, the deflection angle is as small as $\delta\theta \approx 10^{-6} \sim 10^{-7}$. Hence, a large enlargement of the deflection angle still would not “derail” the electron wave off the qubit. Secondly, despite what is just mentioned, suppose that the angular spread in, e.g., x -direction interferes with the operation of qudit y . A possible way to sidestep this problem is to employ the scheme similar to the anamorphotic obstruction-free phase shifter [23] to “pinch” the electron wave, using electron-optical elements similar to ones used in aberration correction. Thirdly, we need multiple millikelvin refrigerators [24], such as the dilution refrigerator or the adiabatic demagnetization refrigerator, to cool the qubits if we use room-temperature electromagnetic lenses between the qubits. Nonetheless, we need only a logarithmic number of refrigerators in terms of d .

Although biological specimens are supposed to be weak-phase objects, transmitted waves are not necessarily smooth. Elastically scattered waves from a number of atoms to the forward direction are roughly in phase and hence the resultant waves are smooth. However, high-angle elastic scattering, up to ≈ 10 mrad, results from addition of waves with essentially random phase values. This entails rapidly fluctuating intensity in the diffraction plane [25]. Hence, this results in a failure of the process in Eq. (2) if the electron is detected in the region of high-angle scattering, because each state $|p, q\rangle$ has different amplitude at the point of detection. Figure 2 (c) shows a workaround for this problem. Waves resulting from high-angle elastic scattering are simply merged with the forward-scattered wave to “obscure the fact” that high-angle scattering ever happened, at the expense of introducing small errors. Versatile electron-wave manipulation methods may be employed to merge those waves [22]. Alternatively, a lens with strong spherical aberration could approximate such a function.

Having discussed hardware designs, we proceed to consider software. In principle, any measurement method physically possible should straightforwardly be imple-

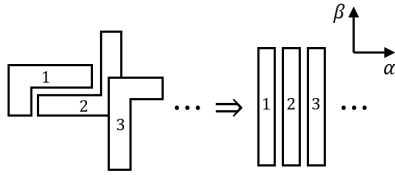


FIG. 3: Grover search for patterns on the specimen. One may try to identify which region, out of regions $1, 2, \dots$ that may overlap, have the large phase shift (left hand side). Within the quantum computer, one may rearrange these regions in a regular fashion, while doing one's best to keep the nearby points in the original space close in the transformed space, in order to be resistant to inelastic scattering.

mented, because of the universality of our scheme. On the other hand, Grover search has not been discussed in the QEM context. Here we define two words to avoid confusion in the following discussions. We call the process described in Eq. (1) an *oracle call*. We refer to a call from “off-the-shelf” Grover algorithm, which expects a zero or π -phase shift, as a *subroutine call*.

The simplest, although artificial, application of Grover’s algorithm is search for an object, or rather a single pixel A. Pixel A has the phase shift π , while all other pixels have zero phase shift. In this case, Grover’s algorithm enables us to find pixel A with \sqrt{N} queries, when there are N pixels in total. If the phase shift is π/k instead of π , then we can let k electrons pass the specimen for each subroutine call from Grover’s algorithm. There is a caveat, however. Since the quantum amplitude at pixel A grows as $\approx \sin\left(\frac{\pi s}{2\sqrt{N}}\right)$ at s -th iteration, the sum of the quantum probability at pixel A through \sqrt{N} iterations is approximately $\int_0^{\sqrt{N}} \sin^2\left(\frac{\pi s}{2\sqrt{N}}\right) ds = \frac{\sqrt{N}}{2}$. On the other hand, if one “classically” measures the phase shift value pixel by pixel, the sum of the probability at pixel A is 1. Hence, the possibility of inducing radiation damage at pixel A is *larger* with Grover search compared to the simple method. Thus, in this particular case Grover search makes sense only when one cares about the specimen damage at *all* pixels, rather than at the pixel we seek.

Grover search does make sense if our task is to seek a pattern. Suppose we have N candidate patterns for the phase map of the specimen, and we want to determine which pattern reflects the true structure of the specimen. Sequential testing would cost $\propto N$ queries, which we want to cut down to $\propto \sqrt{N}$. Consider patterns $1, 2, \dots, N$, as specific areas on the specimen, as on the left-hand side of Fig. 3. We intend to find which of the numbered areas have a strong phase shift. Suppose that the strong phase shift is known to be of the order π/k . Suppose also that each of the numbered areas naturally have weak variations of phase shift within its area. Let the set of spatial points (p, q) comprising α -th candidate pattern be P_α . Our procedure to find the true pattern is

as follows. We begin with a superposition $\sum_{\alpha=1}^N |\alpha\rangle$ and then produce $\sum_{\alpha=1}^N |\alpha\rangle \otimes \left\{ \sum_{(p,q) \in P_\alpha} |p, q\rangle \right\}$. After an oracle call, we obtain $\sum_{\alpha=1}^N |\alpha\rangle \otimes \left\{ \sum_{(p,q) \in P_\alpha} e^{i\theta_{p,q}} |p, q\rangle \right\}$. Since we compute with a QC, we may freely rearrange the points (p, q) to obtain a more regular configuration shown in the right-hand side of Fig. 3. This results in a state

$$\sum_{\alpha=1}^N |\alpha\rangle \otimes \left\{ \sum_{\beta} e^{i\Theta_{\alpha,\beta}} |\alpha\rangle \otimes |\beta\rangle \right\}, \quad (4)$$

where $|\alpha\rangle \otimes |\beta\rangle = |\alpha, \beta\rangle$ and $\Theta_{\alpha,\beta}$ primarily represents the phase shift for the α -th pattern and it weakly depends on β . To extract the mean value $\Theta_\alpha \propto \sum_{\beta} \Theta_{\alpha,\beta}$, we first quantum Fourier transform (QFT) the state of Eq. (4) with respect to β to get the average at the zero-frequency state. Then we multiply i to all nonzero spatial-frequency states to make the phase variation to a less harmful amplitude variation. We then apply inverse-QFT and measure β . This results in

$$\approx \sum_{\alpha=1}^N |\alpha\rangle \otimes e^{i\Theta_\alpha} |\alpha\rangle. \quad (5)$$

Finally, we measure the state of the rightmost ket in Eq. (5) with respect to the Fourier-transformed basis of the form $|\gamma\rangle = \frac{1}{\sqrt{M}} \sum_{\gamma} e^{i\frac{\gamma\alpha}{M}} |\alpha\rangle$. After a phase correction step, we obtain $\sum_{\alpha=1}^N e^{i\Theta_\alpha} |\alpha\rangle$. Hence, we can compose a Grover subroutine call by repeating this process for $\approx k$ times. To be resistant to inelastic scattering, which “mildly collapses” the wavefunction in the real space, we may ensure the followings. Firstly, for any given point A on the specimen, most candidate patterns are designed to include a point that is close to point A. Secondly, the mapping of Fig. 3 is such that measurement of β does not eliminate surviving candidate patterns.

As a final comment, we draw the reader’s attention to quantum algorithms [26, 27] that are able to efficiently find a pattern and report its place. Although these algorithms work only for phase objects with phase shift values known to be 0 or π , they might suggest the existence of useful quantum algorithms in the context of QEM.

In summary, we have shown a simple universal QEM scheme. Also shown is evidence that useful quantum algorithms exist to take advantage of such a QEM. Much theoretical study remains to be done, let alone experimental effort. Useful algorithms should tolerate imprecise “oracles”, inelastic scattering events, and preferably be executable on a noisy intermediate-scale quantum (NISQ) computer.

The author thanks Professor Robert M. Glaeser for discussions on the future of cryoEM. This research was supported in part by the JSPS “Kakenhi” Grant (Grant No. 19K05285).

[1] Peter Hoyer and Robert Spalek, Lower bounds on quantum query complexity, *Bull. EATCS* **87**, 78-103 (2005).

[2] R. M. Glaeser, K. Downing, D. DeRosier, W. Chiu, and J. Frank, *Electron Crystallography of Biological Macromolecules* (Oxford University Press, New York, 2007).

[3] H. Okamoto, Quantum interface to charged particles in a vacuum, *Phys. Rev. A* **92**, 053805 (2015).

[4] H. Okamoto, Resilient quantum electron microscopy, *Phys. Rev. A* **106**, 022605 (2022).

[5] P. Kruit, R. G. Hobbs, C-S. Kim, Y. Yang, V. R. Manfrinato, J. Hammer, S. Thomas, P. Weber, B. Klopfer, C. Kohstall, T. Juffmann, M. A. Kasevich, P. Hommelhoff, and K. K. Berggren, Designs for a quantum electron microscope, *Ultramicroscopy* **164**, 31-45 (2016).

[6] I. Madan, G. M. Vanacore, S. Gargiulo, T. LaGrange, and F. Carbone, The quantum future of microscopy: Wave function engineering of electrons, ions, and nuclei, *Appl. Phys. Lett.* **116**, 230502 (2020).

[7] Stewart A. Koppell, Yonatan Israel, Adam J. Bowman, Brannon B. Klopfer, and M. A. Kasevich, Transmission electron microscopy at the quantum limit, *Appl. Phys. Lett.* **120**, 190502 (2022).

[8] S. A. Koppell, M. Mankos, A. J. Bowman, Y. Israel, T. Juffmann, B. B. Klopfer, and M. A. Kasevich, Design for a 10 keV multi-pass transmission electron microscope, *Ultramicroscopy* **207**, 112834 (2019).

[9] Amy E. Turner, Cameron W. Johnson, Pieter Kruit, and Benjamin J. McMorran, Interaction-Free Measurement with Electrons, *Phys. Rev. Lett.* **127**, 110401 (2021).

[10] H. Okamoto, Possible use of a Cooper-pair box for low-dose electron microscopy, *Phys. Rev. A* **85**, 043810 (2012).

[11] T. Juffmann, S. A. Koppell, B. B. Klopfer, C. Ophus, R. M. Glaeser, and M. A. Kasevich, Multi-pass transmission electron microscopy, *Sci. Rep.* **7**, 1699 (2017).

[12] Dmitry Lyumkis, Challenges and opportunities in cryo-EM single-particle analysis, *J. Biol. Chem.* **294**, 5181-5197 (2019).

[13] Bronwyn A. Lucas, Benjamin A. Himes, Liang Xue, Timothy Grant, Julia Mahamid, and Nikolaus Grigorieff, Locating macromolecular assemblies in cells by 2D template matching with cisTEM, *eLife* **10**:e68946 (2021).

[14] Colin Ophus, Four-Dimensional Scanning Transmission Electron Microscopy (4D-STEM): From Scanning Nanodiffraction to Ptychography and Beyond, *Microsc. Microanal.* **25**, 563-582 (2019).

[15] Morten Kjaergaard, Mollie E. Schwartz, Jochen Braumueller, Philip Krantz, Joel I.J. Wang, Simon Gustavsson, and William D. Oliver, Superconducting Qubits: Current State of Play, *Annu. Rev. Condens. Matter Phys.* **11**, 369-395 (2020).

[16] Hiroshi Okamoto and Yukinori Nagatani, Entanglement-assisted electron microscopy based on a flux qubit, *Appl. Phys. Lett.* **104**, 062604 (2014).

[17] T. Lanting, A. J. Przybysz, A. Yu. Smirnov, F. M. Spedalieri, M. H. Amin, A. J. Berkley, R. Harris, F. Altomare, S. Boixo, P. Bunyk, N. Dickson, C. Enderud, J. P. Hilton, E. Hoskinson, M. W. Johnson, E. Ladizinsky, N. Ladizinsky, R. Neufeld, T. Oh, I. Perminov, C. Rich, M. C. Thom, E. Tolkacheva, S. Uchaikin, A. B. Wilson, and G. Rose, Entanglement in a Quantum Annealing Processor, *Phys. Rev. X* **4**, 021041 (2014).

[18] Hiroshi Okamoto, Full-vortex flux qubit for charged-particle optics, *Phys. Rev. A* **97**, 042342 (2018).

[19] Brian Vlastakis, Gerhard Kirchmair, Zaki Leghtas, Simon E. Nigg, Luigi Frunzio, S. M. Girvin, Mazyar Mirrahimi, M. H. Devoret, R. J. Schoelkopf, Deterministically Encoding Quantum Information Using 100-Photon Schroedinger Cat States, *Science* **342**, 607-610 (2013).

[20] Hiroshi Okamoto, Reza Firouzmand, Ryosuke Miyamura, Vahid Sazgari, Shun Okumura, Shota Uchita, Ismet I. Kaya, TEM at millikelvin temperatures: Observing and utilizing superconducting qubits, *Micron* **161**, 103330 (2022).

[21] Robert Zimmermann, Michael Seidling, and Peter Hommelhoff, Charged particle guiding and beam splitting with auto-ponderomotive potentials on a chip, *Nat. Commun.* **12**, 390 (2021).

[22] Marius Constantin Chirita Mihaila, Philipp Weber, Matthias Schneller, Lucas Grandits, Stefan Nimmrichter, and Thomas Juffmann, Transverse electron-beam shaping with light, *Phys. Rev. X*, in press. (2022).

[23] H. Rose, Theoretical aspects of image formation in the aberration-corrected electron microscope, *Ultramicroscopy* **110**, 488-499 (2010).

[24] P. Magnard, S. Storz, P. Kurpiers, J. Schaer, F. Marxer, J. Luetolf, T. Walter, J.-C. Besse, M. Gabureac, K. Reuer, A. Akin, B. Royer, A. Blais, and A. Wallraff, Microwave Quantum Link between Superconducting Circuits Housed in Spatially Separated Cryogenic Systems, *Phys. Rev. Lett.* **125**, 260502 (2020).

[25] Hiroshi Okamoto, Measurement errors in entanglement-assisted electron microscopy, *Phys. Rev. A* **89**, 063828 (2014).

[26] G. Kuperberg, A subexponential-time quantum algorithm for the dihedral hidden subgroup problem, *SIAM J. Comput.* **35**, 170-188 (2005).

[27] Ashley Montanaro, Quantum Pattern Matching Fast on Average, *Algorithmica* **77**, 16-39 (2017).